ACS Partner Journal

Journal of the American Society for Mass Spectrometry

pubs.acs.org/jasms

Article

Enhancing Top-Down Analysis of Proteins by Combining Ultraviolet Photodissociation (UVPD), Proton-Transfer Charge Reduction (PTCR), and Gas-Phase Fractionation to Alleviate the Impact of Nondissociated Precursor Ions

Sean D. Dunham and Jennifer S. Brodbelt*

Cite This: *J. Am. Soc. Mass Spectrom.* 2024, 35, 255−265

Read Online

ACCESS | Metrics & More | Article Recommendations | Supporting Information

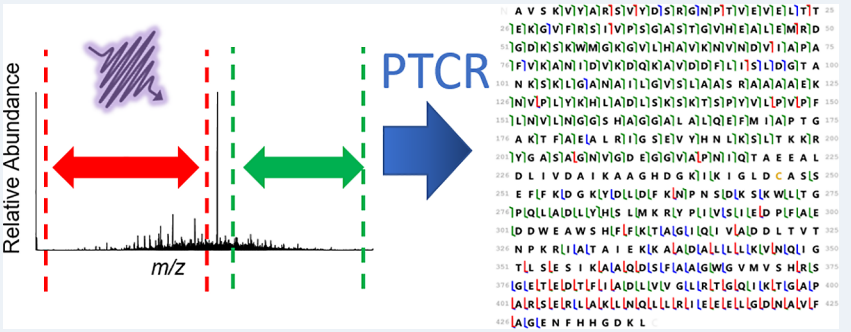

ABSTRACT: Recent advances in top-down mass spectrometry strategies continue to improve the analysis of intact proteins. 193 nm ultraviolet photodissociation (UVPD) is one method well-suited for top-down analysis. UVPD is often performed using relatively low photon flux in order to limit multiple-generation dissociation of fragment ions and maximize sequence coverage. Consequently, a large portion of the precursor ion survives the UVPD process, dominates the spectrum, and may impede identification of fragment ions. Here, we explore the isolation of subpopulations of fragment ions lower and higher than the precursor ion after UVPD as a means to eliminate the impact of the surviving precursor ion on the detection of low abundance fragment ions. This gas-phase fractionation method improved sequence coverage harvested from fragment ions found in the m/z regions lower and higher than the precursor by an average factor of 1.3 and 2.3, respectively. Combining this gas-phase fractionation method with proton transfer charge reduction (PTCR) further increased the sequence coverage obtained from these m/z regions by another factor of 1.3 and 1.4, respectively. Implementing a post-UVPD fractionation + PTCR strategy with six fractionation events resulted in a sequence coverage of 75% for enolase, the highest reported for 193 nm UVPD.

INTRODUCTION

Top-down mass spectrometry offers an exciting opportunity to identify and characterize intact proteins, thus bypassing the use of proteolysis common to bottom-up proteomics methods. The increasing access to high-resolution mass spectrometers, such as Orbitrap,[1,2] FT-ICR,[3] and Q-TOF[4,5] mass spectrometers, has accelerated the adoption of top-down methods. One notable advantage of top-down strategies is that they offer the potential characterization of combinatorial patterns of post-translational modifications (PTMs) not possible with bottom-up strategies owing to the inability to map multiple PTMs based on analysis of short peptides.[3,6,7] Despite the prospects for complete characterization of all proteins and their multitude of proteoforms, the promise of top down analysis remains only partially fulfilled owing to limitations in activation/dissociation methods, high resolution separation techniques, and sensitivity issues associated with the broad dynamic range of protein concentrations and the stoichiometries of PTMs.

There have been significant inroads in developing new activation modes to increase the production of fragment ions from proteins,[6,8,9] and an equally important effort has been directed at harvesting more information from the resulting fragmentation patterns. The performance of virtually all activation methods degrades with the increasing mass of the protein, in part due to insufficient internal energy deposition and in part due to the inability to assign all fragment ions. In general, higher energy methods of activation such as electron-based activation methods (electron capture dissociation (ECD) or

Received: October 5, 2023
Revised: December 5, 2023
Accepted: December 11, 2023
Published: December 27, 2023

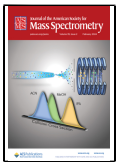

electron transfer dissociation (ETD))[10−13] and ultraviolet photodissociation (UVPD)[14−17] have been shown to provide a greater degree of protein characterization compared to collisional-based methodologies, particularly for larger proteins. Addition of supplemental activation to electron-based methods, such as electron transfer higher-energy collisional dissociation (EThCD) or activated ion electron transfer dissociation (AI-ETD), counters the impact of the prevalent charge-reduction/no dissociation pathways, and has improved the ability to sequence and characterize larger proteins.[13,16,18] UVPD generates a variety of fragment ion types (a/x, b/y, and c/z)[14,19−21] which offers great potential for comprehensive characterization of proteins, yet at the same time results in dense spectra and decreased signal-to-noise because the ion current is dispersed among so many fragmentation pathways. All of these MS/MS methods also produce multiple-generation fragment ions, particularly internal ions,[12,22] that increase in abundance and number when the activation conditions are modified to attain higher energy deposition.[23,24] A common conundrum of top-down analysis is that extensive fragmentation is needed to fully characterize protein sequences, identify mutations, and pinpoint sites of PTMs, yet at the same time the most dense, information-rich spectra often suffer from production of redundant fragment ions in multiple charge states and from overlapping isotope patterns of fragment ions, making them unassignable. Furthermore, achieving the highest sequence coverage to maximize the characterization of large proteins requires significant spectral averaging, a factor that confounds high throughput analysis required for LC time scales. In summary, three of the key limitations related to production and interpretation of MS/MS spectra of large intact proteins are spectral congestion, poor ion statistics, and, uniquely for ion trapping platforms, charge capacity limitations.

Many of the factors that mediate the information content of MS/MS spectra of intact proteins are related to the balance between producing informative fragmentation patterns and mitigating spectral congestion. Proton transfer charge reduction (PTCR) reactions have proven to be highly successful for combatting spectral congestion in ion trapping instruments.[25−29] PTCR entails the reaction of reagent anions with multicharged analyte ions of interest to charge reduce and disperse analyte ions over a broader m/z space, reducing spectral congestion that may obscure less abundant ions or prevent confident assignment owing to overlapping isotopic profiles.[30] PTCR has been performed following ETD and UVPD in numerous applications and has enhanced the degree of characterization of intact proteins.[22,24,26,28,31−33] PTCR has been shown to allow more accurate and reliable deconvolution of internal fragment ions.[22] However, PTCR also may diminish the abundance of fragment ions by diluting their signals across multiple charge states. To counter this issue, ion parking[32] can be performed. Ion parking entails applying an auxiliary waveform during PTCR to excite ions of a particularly frequency range, increasing their kinetic energies and suppressing further PTCR. Parking allows ions to be concentrated in fewer or single charge states.[29,34,34−36] Most recently, this powerful PTCR-parking strategy has been applied on a 21 T FT-ICR platform to showcase the analysis of proteins from cell lysates in an LCMS workflow.[27] Based on MS1 information alone, the number of proteoforms increased from 1404 to 2472 as a consequence of both reduced spectral congestion and consolidation of ion signal.[27] Additionally, on Orbitrap platforms, large highly charged proteins often exhibit low S/N which is attributed to their inability to survive the full length of the transient acquisition.[37] In this context, PTCR reduces the charge states of proteins and consequently improves S/N due to longer survival times in the Orbitrap analyzer.[37] PTCR has also been performed as a means of gas-phase fractionation via isolation of "slices" of MS1 spectra acquired during an LC run and subjecting ions to PTCR prior to CID and HCD, enabling the identification of additional proteoforms.[38]

As protein size increases, the number of potential fragmentation pathways increases, diminishing the probability of observing any particular fragment ion. Furthermore, higher energy deposition may cause the formation of multiple-generation product ions (i.e., consecutive fragmentation), a process that can degrade large fragment ions and diminish coverage in the center sequence section of proteins. Auxiliary methods have been developed to counter the generation of multiple-generation product ions during IRMPD,[39] UVPD,[23,40] and ETD[24,41] in ion traps. These methods involve the application of low amplitude broadband dipolar excitation waveforms in which frequencies corresponding to the precursor ions are omitted, allowing selective excitation of fragment ions in a manner that either moves them away from the path of the laser (for photodissociation methods) or selectively quenches the reaction of fragment ions with reagent anions during ETD. This strategy when applied during UVPD has been coined fragment ion protection (FIP) and has both increased the S/N of fragment ions and improved the center sequence coverage of large proteins.[23,40] Advantages of such auxiliary strategies for top-down analysis have also been highlighted when implemented during ETD, as described for tailored parallel ion parking during ETD (PIP-ETD).[24] In one of the PIP-ETD applications, both tailored waveforms for PIP and PTCR were performed following ETD.[24] PIP-ETD improved the sequence coverage of protein G (21 kDa) from 80% to 91%.[24] More notably, the number of complementary ion pairs increased from 39% with standard ETD to 91% with PIP-ETD, reflecting the decreased production of multiple-generation ETD ion products.[24] Performing multiple injections of fragment ions in a storage cell, a process known as "multi-fills", prior to the analysis of the entire collection has been explored as another means of enhancing fragment ion populations and improving S/N.[31,42,43] Another strategy, termed chimeric ion loading, entails accumulation of fragment ions generated from both CID and ETD prior to detection, leading to an average sequence coverage of 33% for proteins derived from a MCF7 lysate as compared to 15% and 23% for CID and ETD, respectively, without chimeric ion loading.[43]

Ion trapping mass spectrometers have charge capacity limitations that constrain the population of ions, whether intact proteins or fragment ions. As proteins increase in size, they typically carry more charges, meaning a lower number of protein ions can be accumulated without exceeding the charge capacity of the mass analyzer. The population of fragment ions created upon activation of protein faces similar constraints, a factor exacerbated upon formation of hundreds of different fragment ions in multiple charge states. Gas-phase fractionation strategies have been used in several applications to subdivide the m/z range in order to consolidate more charges (i.e., more ions) in specific m/z regions.[44−46] These fractionation methods have yielded higher S/N of lipids[44] and peptides[45,46] in complex mixtures. An alternative fractionation concept has been implemented via field asymmetric waveform ion mobility spectrometry (FAIMS) to fractionate ions across multiple runs

https://doi.org/10.1021/jasms.3c00351
J. Am. Soc. Mass Spectrom. 2024, 35, 255−265

as a result of mobility differences, as demonstrated for peptides in lysates.[47,48]

As ion populations exceed the capacity of ion traps, space charging results in decreased mass accuracy owing to Coulombic repulsion of ions. Particularly in the context of top down analysis using UVPD as the MS/MS method, large precursor ion populations are used to maximize the abundances of fragment ions while at the same time limiting the laser fluence or photon flux to avoid the formation of multiple-generation product ions. The use of a low laser fluence results in survival of a large portion of the precursor ion. At the same time, it has been noted that an ion packet of large abundance in an Orbitrap analyzer can cause more rapid decay of other lower abundance ions of similar m/z, degrading the S/N of the latter.[49] To mitigate the effects of space charging, the nondissociated precursor may be ejected after UVPD by application of an additional waveform.[50,51] In one application both the S/N and mass accuracy of peptide fragment ions were improved when using this precursor ejection process following 193 nm UVPD of peptides in a linear ion trap mass spectrometer.[50] More recently, an MS^3 precursor exclusion strategy was developed on an Orbitrap platform for the analysis of unsaturated glycerophospholipids, resulting in up to a 13X increase in the S/N of diagnostic fragment ions.[51] Gains in S/N were attributed to minimization of both space charging in the Orbitrap analyzer and dephasing of low abundance fragment ions caused by the presence of the highly abundant precursor ion population.[49,52]

This collection of findings related to PTCR and gas-phase fractionation methods provides insight into the types of strategies that should yield dividends for improving top-down methods for protein analysis. In particular, the current study focuses on improving the S/N of fragment ions generated by UVPD of intact proteins by combining PTCR and gas-phase fractionation in an Orbitrap mass spectrometer. As presented here, isolating multiple "windows" of fragment ions both lower and higher than the m/z of the precursor ion prior to PTCR affords notable benefits. We propose that the gains in signal are in part due to overcoming charge capacity limitations of the C-trap and alleviating the deleterious impact of an abundant nondissociated precursor ion on the detection of fragment ions in the higher m/z region.

EXPERIMENTAL SECTION

Materials. Lyophilized bovine carbonic anhydrase II (29 kDa, 259 amino acids), aldolase from rabbit muscle (39 kDa, 363 amino acids), enolase from baker's yeast (46 kDa, 436 amino acids), and protein AG(50 kDa, 454 amino acids) were purchased from Millipore Sigma and dissolved in 50% methanol with 0.1% formic acid at a concentration of 10 uM. Each solution was directly infused into the mass spectrometer using a heated ESI (HESI) source at a flow rate of 3−5 ul/min and using applied voltages ranging from 3.2−5.0 kV.

Mass Spectrometry. Experiments were performed on a Thermo Fisher Scientific Orbitrap Fusion Lumos Tribrid mass spectrometer (San Jose, CA) modified to implement 193 nm UVPD in the dual linear ion trap using a 500 Hz excimer laser (Coherent Excistar XS) as described previously.[53] The mass spectrometer was also modified to enable proton transfer charge reduction (PTCR) using the reagent perfluoroperhydrophenanthrene (PFPP), similarly to that described previously.[29,38] For PTCR, reaction conditions were varied as needed to reduce the charge states of fragment ions and thus disperse them up to a range of m/z 3000−3500. The PTCR reaction time varied from 25 to 200 ms and utilized a reagent q value of 0.45. In some cases, multiple rounds of charge reduction were performed by repeated injections of the PFPP reagent ion (2e5 charges), a method described previously.[54] UVPD was performed in the high pressure trap (HPT) of the dual linear ion trap with one pulse and a laser energy of 0.5−1.0 mJ. Specifically, for carbonic anhydrase UVPD was performed with 1.0 mJ, whereas a laser energy of 0.5 mJ was used for all other proteins unless specified otherwise. The pressure in the ion routing multipole was reduced to 0.002 Torr to optimize transmission and detection of fragment ions. UVPD mass spectra were collected using a resolution of 240 000 at m/z 200, an automatic gain control target (AGC) of 5e5 charges, the mass range set to high, and full profile mode. 100−900 transient averages were collected for experiments depending on the experimental comparison. For the fractionation method, ion populations were sectioned based on specific ranges of m/z values, and the sectioning was implemented by broadband isolation using appropriate combinations of DC and RF voltages enabled by the MS^n feature of the standard instrument control software. Additional details are included in Supporting Information. Fractionation windows lower in m/z than the precursor were offset by 2 m/z. Windows directly higher in m/z than the precursor were offset by 15 m/z to avoid collisional excitation of the precursor that may occur when the window is set closer, resulting in inadvertent CID. For all fractionation strategies, adjacent fractionation windows overlapped by 5 m/z to ensure capture of fragments ions at the edges of windows.

Data Analysis. FreeStyle Xtract was used to deconvoluted mass spectra using a fit factor of 70% and S/N threshold of 10 with consideration of overlap. ProSight Lite was used to match fragment ions to deconvoluted mass lists with a mass error tolerance of 10 ppm. To streamline data analysis, $a/a+1$ ions were grouped together, as were $y/y-1$ and $x/x+1$ ions. When specified, fragment ion masses were only retained if identified in two of three replicates as a means to filter out potential spurious masses and improve confidence in assignments. Fragment ion isotope distributions were simulated using the averagine model and a script in Matlab. Noise levels in mass spectra were determined by plotting the distribution of signal and setting the noise level as the upper edge of the noise distribution, as determined with the second derivative of the signal distribution.[55,56] A detailed discussion of noise features of the spectra is included in Supporting Information (SI) along with Figures S1−S4. The data and the list of matched fragment ions are available in the jPOST repository under accession numbers JPST002408

DISCUSSION AND RESULTS

Past studies that have shown the benefits of precursor ejection[50] or precursor exclusion[51] following UVPD. Elimination of the abundant surviving precursor can be accomplished by using a selective precursor ejection waveform[50] or using an MS^3 method to isolate the fragment ion population without retaining the precursor ions.[51] Specific subsets of the fragment ion population can be targeted using multiple isolation events, a process termed post-UVPD fractionation (PUF). Excluding the precursor through PUF is expected to achieve a similar outcome to precursor ejection. Both methods were evaluated for the top-down analysis of proteins in the present study. Results based on the precursor ejection method and comparisons to PUF are described in SI ("Evaluation of Precursor Ejection" and Figures S5−S7). Because the performance metrics of PUF surpassed

https://doi.org/10.1021/jasms.3c00351
J. Am. Soc. Mass Spectrom. 2024, 35, 255−265

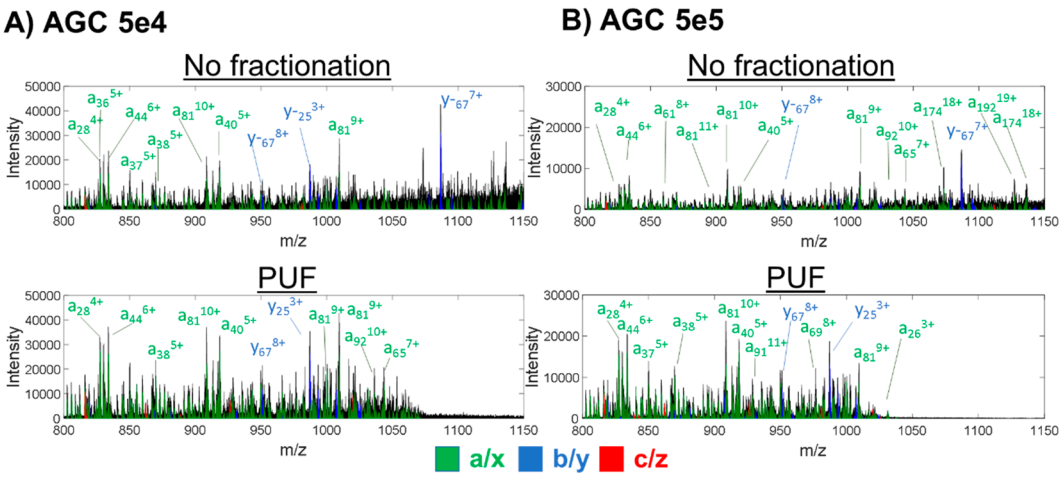

Figure 1. Representative sections of UVPD mass spectra (1.0 mJ, one pulse) of carbonic anhydrase (25+, m/z 1161) without or with PUF using a window of m/z 159−1159 and AGC targets of (A) 5e4 or (B) 5e5. Spectra were collected with 100 transient averages. Theoretical isotope distributions of identified fragment ions are overlaid on the mass spectra, scaled with the intensity value provided by Xtract, and color-coded for fragment ion type. Prominent fragment ions are annotated.

that of precursor ejection, the former was adopted for the remainder of the present study.

To demonstrate the impact of PUF on the MS/MS spectra of intact proteins, UVPD spectra were acquired without and with fractionation using carbonic anhydrase (25+, m/z 1161.9) as a representative protein. After UVPD, fractionation using 1000 m/z windows both lower (m/z 159−1159) and higher (m/z 1176−2176) than the precursor ion was performed, and examples of the resulting spectra are shown in Figure S8. Gains in signal were observed for m/z regions lower and higher than the precursor ion. The sequence coverage obtained from the m/z region lower than the precursor increased from an average of 62% (UVPD alone) to 69% (PUF), and a gain of 20% coverage was obtained for the m/z region higher than the precursor ion (23% for UVPD alone to 43% for PUF).

The performance metrics of ion traps are known to depend on the size of the ion population as defined by the total number of charges. The C-trap charge capacity has been reported to be lower than that of the linear ion trap (where UVPD is performed prior to transfer of ions to the C-trap for bunching and then pulsed into Orbitrap for high resolution analysis),[57] and thus the C-trap is expected to have a significant impact on charge capacity effects on ion analysis. To explore whether gains in signal when coupling UVPD with fractionation are in part due to overcoming C-trap charge capacity limitations, UVPD spectra were collected for carbonic anhydrase (25+, m/z 1161.9) while varying the size of the ion population, as defined by the automatic gain control (AGC) target (5e4 to 1e6). Based on measurement of signal level in a prescan, the automatic gain control feature regulates the number of ions in an ion trap to mitigate space charge effects. UVPD mass spectra were acquired without fractionation using 1000 m/z windows both lower (m/z 159−1159) and higher (m/z 1176−2176) than the precursor ion. Signal increases were observed for the PUF spectra for each AGC target, as illustrated for an excerpt of the lower m/z window in Figure 1 (and Figure S9 for the higher m/z window). The increase was more substantial for the larger AGC target of 5e5 for which charge capacity limitations of the C-trap are expected to play a larger role. Despite the overall increase in signal, a swath of fragment ions lower in m/z than the precursor was lost when performing PUF at an AGC target of 5e5. Furthermore, this effect seems to be exaggerated for higher AGC targets, suggesting that space charging plays a role in the loss of ions. Reduction of the isolation window from 1000 m/z to 750 m/z to 500 m/z *to* 250 m/z decreased the swath of lost fragment ions as displayed in Figure S10. In total, 57 ± 3 unique fragment ions lower in m/z than the precursor were identified without fractionation, and 110 ± 4 were identified when performing PUF of the window spanning 1000 m/z lower than the precursor (for UVPD of carbonic anhydrase (25+, m/z 1161) with an AGC target of 5E5). When comparing the fragment ions identified lower in m/z than the precursor for the spectra acquired using PUF and no fractionation, 136 ± 4 ions were found in common. Despite the loss of fragment ions lower in m/z than the precursor when applying PUF using wide fractionation windows, overall more fragment ions are identified following PUF and the overall loss of ions can be tempered by utilization of smaller isolation windows.

Sequence coverages were calculated for carbonic anhydrase (25+) based on the resulting UVPD spectra without and with fractionation, as summarized in Figure 2 for 1000 m/z windows lower and higher than the precursor ion at AGC targets of 5e4 to 1e6. Regardless of the AGC target, sequence coverage increased by 7−20% with fractionation, and gains in sequence coverage were particularly evident for the m/z window higher than precursor. Additionally, despite the loss of fragment ions lower in m/z than the precursor when using the PUF approach, sequence coverage still increased, suggesting some of the lost fragment ions were redundant ones. Sequence coverage generally plateaued at an AGC target of 5e5, suggesting saturation of the ion population in the C-trap. Thus, an AGC target of 5e5 was used for the remainder of the study.

Prior to fractionation, the surviving precursor ion is the most abundant ion in the UVPD spectra. The fractionation process ejects the precursor ion from the population of trapped ions, thus alleviating its impact on the storage, transfer, and detection of all other ions owing to alleviation of space-charging and dephasing of ions of lower abundance. Ion distributions have been previously modeled for RF flatapoles (an ion guide/ion storage device), revealing that ions of lower m/z push ions of higher m/z to the outer edges of the ion bundle.[58] Based on this model, the abundant surviving precursor after UVPD may inhibit the detection of species of a higher m/z upon injection

https://doi.org/10.1021/jasms.3c00351
J. Am. Soc. Mass Spectrom. 2024, 35, 255−265

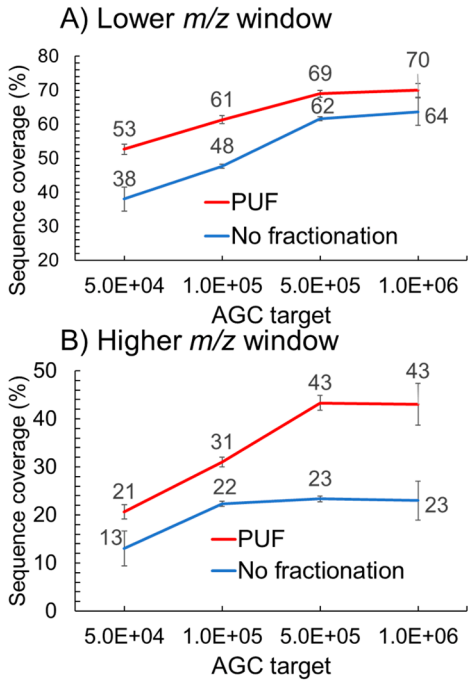

Figure 2. Sequence coverage obtained from UVPD mass spectra (1.0 mJ, one pulse) acquired for carbonic anhydrase (25+, m/z 1161) without or with PUF using a (A) lower window of m/z 159−1159 and (B) higher window of m/z 1176−2176 and a variety of AGC targets. Spectra were collected with 100 transients averaged. The graphs show the sequence coverages harvested from the lower or higher windows (not combined).

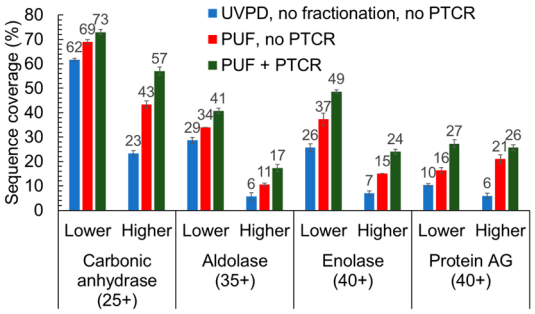

Figure 3. Sequence coverages from fragment ions derived from m/z regions lower and higher than the precursor ion obtained for carbonic anhydrase (25+, m/z 1161), aldolase (35+, m/z 1121) enolase (40+, m/z 1167), and protein AG (40+, m/z 1262) by UVPD (0.5−1.0 mJ, one pulse) without PUF, with PUF, and with PUF + PTCR. Fractionation utilized 1000 m/z windows lower and higher than the precursor ion. PTCR was performed on each fractionation window with conditions optimized to disperse fragment ions to m/z 3000−3500. All spectra were collected with 100 transients averaged. Summation of the sequence coverages from the lower and higher m/z regions may exceed 100% owing to redundant fragment ions found in both regions.

from the C-trap to the Orbitrap analyzer, rationalizing the more significant gains in sequence coverage obtained from fragment ions in the higher m/z window compared to the lower window.

PUF and PTCR. PUF was also explored for other larger proteins, including aldolase (35+, m/z 1121), enolase (40+, m/z 1167), and protein AG (40+, m/z 1262), using 1000 m/z fractionation windows lower and higher than the precursor. This fractionation process was also combined with PTCR in order to capitalize on the potential gains from alleviation of space charging and dephasing and at the same time dispersing the fragment ions across a broader m/z landscape to alleviate spectral congestion. To accomplish this objective, the fragment ions found in the same m/z windows employed for fractionation were subjected to PTCR, resulting in the strategy referred to as PUF + PTCR. PTCR conditions were varied to disperse the majority of fragment ions up to the m/z range of 3000−3500. The sequence coverages derived from the m/z ranges lower and higher than the precursor without fractionation, with fractionation, and with fractionation and PTCR are summarized in Figure 3. Sequence coverage in all cases improved with fractionation alone and even more with the addition of PTCR. The fact that sequence coverage improved with fractionation alone suggesting that benefits from typical PTCR workflows are in part derived from fractionation of the ion populations. Fractionation on average improved sequence coverage harvested from the m/z region lower than the precursor by a factor of 1.3 and the region higher than the precursor by 2.3. These trends lend further support to the postulate that the highly abundant surviving precursor ion especially suppresses the detection of ions above it in m/z space. Furthermore, combining PTCR and fractionation on average improved the sequence coverage by another factor of 1.3 and 1.4 for the lower and upper m/z windows, respectively, suggesting the higher window may suffer from a greater degree of spectral congestion and thus particularly benefits from PTCR to disperse overlapping fragment ions.

UVPD of intact proteins generates hundreds of fragment ions, many of which are not identified and are attributed to internal ions or fragment ions associated with side-chain losses or other small neutral losses. In general, the percentage of fragments explained for UVPD of intact proteins decreases as protein size increases. For instance, the average percentages of fragments explained for UVPD (without fractionation or PTCR) of carbonic anhydrase (25+), aldolase (35+), enolase (50+), and protein AG (40+) were 18%, 9%, 9%, and 5%, respectively (based on 100 transient averages). However, these metrics improved following fractionation and PTCR as summarized in Figure S11. The gains were particularly notable for the lower m/z fractionation window for which the percentage of fragments explained was as high as 40% for enolase (40+) with fractionation alone and increased to 56% upon addition of PTCR. These trends suggest that the accuracy of deconvolution of fragment ions is enhanced with fractionation and PTCR, thus facilitating confident assignment of ions.

To further evaluate the impact of PUF on alleviating false positive identifications, sequence coverages with fractionation and PTCR were calculated with the additional constraint of only including fragment ions if identified in at least two of three replicates (all based on mass lists of deconvoluted fragment ions). This constraint should reduce the number of spurious fragment assignments by requiring replication of ions. For this evaluation, the percentage of sequence coverage retained using this two-of-three replication constraint relative to average sequence coverage obtained per singlicate is tabulated in Table S1. The sequence coverage retained was larger for the lower m/z window in all cases but protein AG, where spectral congestion was notably greater for the lower m/z window in comparison to the higher m/z window, unlike the other proteins in this study. Furthermore, the percentage sequence coverage retained increased by 3−30% for all proteins when combining fractionation with PTCR (with the lone exception again noted for the higher m/z window for protein AG). This general

https://doi.org/10.1021/jasms.3c00351
J. Am. Soc. Mass Spectrom. 2024, 35, 255−265

outcome is consistent with the expectation of the alleviation of false positive assignments of fragment ions upon reduction of spectral congestion. The findings here motivated the adoption of this two-of-three replication constraint for confirmation of fragment ions for the remainder of the study.

PUF + PTCR Strategies. PTCR strategies commonly fractionate ions in selected m/z regions of mass spectra prior to PTCR to focus the charge reduction reactions on smaller populations of ions and obtain more impressive alleviation of spectral overlap when compared to performing PTCR on the entire ion population.[26,28] Fractionation PTCR strategies are particularly advantageous in cases when the reagent anion population is limited or insufficient to achieve the optimal level of charge reduction of highly charged ions. More substantial PTCR can also be accomplished by using multiple injections of the reagent anion population. To further optimize the fractionation and PTCR methods for different end-goals, three strategies were explored in more detail. First, the PUF + PTCR method was refined by modulation of the sizes and number of fractions, employing either two 1000 m/z windows lower and higher than the precursor (as described earlier in this study; this is Strategy 1) or alternatively six windows of variable size (e.g., four 150 m/z windows close to the precursor and two wider windows encompassing the remainder of the m/z range explored with the two window strategy; this is Strategy 2). A schematic of this latter strategy is displayed in Figure S12. Smaller m/z windows were used around the precursor with the expectation of higher spectral density in these regions, thus requiring more targeted PTCR for decongestion. The third strategy, Post-UVPD PTCR double-stage fractionation, entailed isolating 1000 m/z windows both lower and higher than the precursor for PTCR, followed by three additional fractionation events to subdivide each of the two broad windows into three sections for a total collection of six spectra. A schematic of this strategy is described in Figure S13. Though time intensive, this third strategy was explored to see if even more fragment ions would be uncovered by careful manipulation of ion populations. To afford fair comparisons of each method, the total number of transient averages were equated across all spectra.

The isotope patterns of several large fragment ions produced from enolase using the PUF + PTCR two window strategy are displayed in Figure S14, ranging in size from 20 to 38 kDa including x_{187}^{10+}, z_{288}^{13+}, and z_{363}^{14+}, among others. The theoretical isotope distributions and fit percentages scores are provided to show the quality of the fragment ions. Many of the large fragments with low abundances do not exhibit ideal Gaussian-like isotope distributions despite being identified with a strict fit factor requirement of >70%. The observed mismatch of some of the isotope patterns reinforced the requirement that ions be identified in multiple replicates to increase confidence in assignments.

For each method, deconvoluted mass lists from each fractionation window were combined prior to calculating sequence coverage while maintaining the constraint that fragment ions were only retained if present in two of three replicates to reduce spurious assignments. The sequence coverages calculated for each of the three fractionation strategies and numbers of deconvoluted fragment ions are displayed in Figure S15A and S15B, respectively. The PUF + PTCR two-window strategy achieved the highest sequence coverages, ranging from 48% for protein AG to 94% for carbonic anhydrase, outperforming the other two strategies by a small margin− 1% to 6% enhancement depending on the protein. However, upon closer inspection, the PUF + PTCR six-window strategy identified on average 30 additional deconvoluted fragment ions for aldolase, enolase, and protein AG, as tabulated in Figure S15B. These fragment ions may correspond to redundant ion types originating from cleavages at same backbone position (e.g., a_{40} and b_{40}) and thus do not necessarily contribute additional sequence coverage. The post-UVPD PTCR double-stage fractionation strategy outperformed the other methods for one protein, aldolase.

Sequence coverage maps obtained using each fractionation + PTCR strategy are summarized in Figure S16. The six-window fractionation strategy generally identified more fragment ions than the two-window method, but the gain was more substantial for a smaller protein like carbonic anhydrase compared to a larger protein, such as enolase. For example, the six window strategy increased the number of unique fragment ions by 100 for carbonic anhydrase and 17 for enolase. Compared to the two-window method, the six-window strategy also increased the number of redundant fragment ions, those originating from the same backbone position, from 45 to 70 for carbonic anhydrase. For the larger proteins like enolase, fragment ions are more likely to be lower in abundance and larger in size than ones produced from carbonic anhydrase, solely because of the greater number of backbone positions that can be cleaved. Thus, identification of fragment ions from the larger proteins benefited from the more substantial signal averaging of each spectrum for the two-window strategy, and the greater anticipated dispersion of fragment ions using the six-window strategy did not result in notable gains.

Because the differences in the number of unique fragment ion identifications between the PUF + PTCR two-window and six-window strategies were not as pronounced as expected for the large proteins, these comparisons were repeated for enolase (40+) by averaging 1800 transients for sets of spectra as opposed to 600 transients. Collection of 1800 transients requires approximately 1591 s (>26 min) and was anticipated to increase the sequence coverage owing to increased signal-to-noise by a factor of the square root of the number of averages. The expected gains in S/N may be tempered by loss of fragment ions that do not survive the full transient. For both the two-window and six-window strategies, a sequence coverage of 75% was obtained using 1800 transients (compared to 67% for two-window and 62% for six-window using 600 transients) and the number of unique fragment ions increase from 530 for two-window method to 664 for six-window method. The resulting sequence coverage map for enolase (40+) using the PUF + PTCR two-window strategy is displayed in Figure 4. Based on this survey of outcomes, the remainder of the study will utilize the PUF + PTCR two-window strategy with 600 total transients.

For top down analysis of three of the largest proteins in the present study, the number of deconvoluted fragment ions identified using the post-UVPD PTCR double-stage fractionation strategy was greater than the PUF + PTCR two window strategy for the majority of proteins (Figure S15B). The gains using the double-stage fractionation method seem to be largely related to increases in signal intensities of fragment ions. To illustrate the enhancement of signal abundance for enolase (40+), the spectrum obtained via PUF + PTCR two-window method was overlaid with the corresponding spectrum obtained by post-UVPD PTCR double-stage fractionation in Figure 5. Additional comparisons are shown for carbonic anhydrase (25+) and protein AG (40+) in Figure S17A and S17B, respectively. Gains in intensity were further explored by

https://doi.org/10.1021/jasms.3c00351
J. Am. Soc. Mass Spectrom. 2024, 35, 255−265

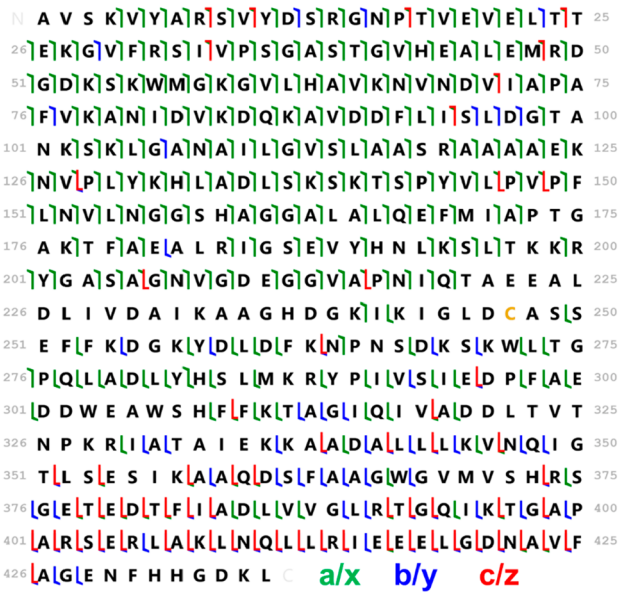

Figure 4. Sequence coverage map based on UVPD (0.75 mJ, one pulse) of enolase (40+, m/z 1167) using the PUF + PTCR two window strategy. Individual spectra were collected with 900 transient averages, thus totaling 1800 transients for the complete set. Fragment ions were only retained if identified in at least two of three replicates. The total sequence coverage is 75%.

summing the intensities of all identified fragment ions derived from the fractionation windows lower and higher than the precursor using either the PUF + PTCR two-window or post-UVPD PTCR double-stage fractionation methods (Figure S18). In all cases, the summed intensities of identified fragment ions were greater using double-stage fractionation, indicating that the double-stage fractionation method best alleviates space charging and dephasing of lower abundance ions.

Prevalence of N-Terminal or C-Terminal Fragment Ions and Coverage of the N-Terminal and C-Terminal Halves of the Proteins. Fractionation windows lower than the m/z of the precursor ion following UVPD often exhibited a higher proportion of N-terminal fragments (a,b,c) relative to C-terminal fragments (x,y,z), while the reverse trend was observed for the fractionation windows higher than the precursor (i.e., more C-terminal fragments). These trends are evident in sequence coverage maps created based on PUF + PTCR for the four proteins in this study (see Figure S19). The percentage of N-terminal and C-terminal fragment ions for the two fractionation windows without and with PTCR are tabulated in Table S2. For example in PUF spectra of enolase, 75% of identified fragment ions in the lower window were comprised of N-terminal fragments (a,b,c), while 76% of identified fragment ions in the higher window were C-terminal fragment ions (x,y,z). Additionally, the average m/z values of N-terminal and C-terminal fragment ions were calculated for spectra obtained using PUF without PTCR (Table S3). On average, C-terminal ions had higher m/z values than N-terminal ions. For instance, for carbonic anhydrase (25+) the average m/z values of N-terminal and C-terminal ions were 850 ± 200 and 1200 ± 400, respectively. The average m/z values of fragment ions of the other proteins are tabulated in Table S3.

Another related trend about the characterization of proteins using top-down methods is that the sequence coverage of the C-terminal regions of large proteins by UVPD is often subpar. Coverage of the C-terminal half of the protein is dominated by C-terminal fragment ions (x,y,z), just as coverage of the N-terminal half of the protein is dominated by N-terminal fragment ions (a,b,c). Since many C-terminal ions are located in the m/z region higher than the precursor ion (per Tables S2 and S3), the

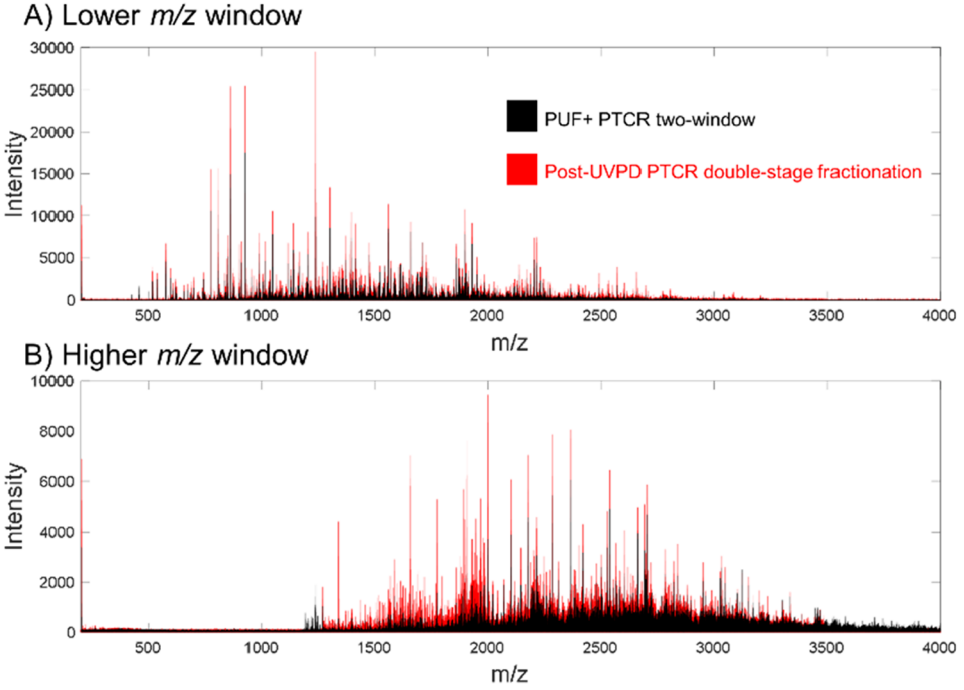

Figure 5. UVPD spectra (0.5 mJ, one pulse) of enolase (40+, m/z 1167) using PUF + PTCR two-window strategy (black) and post-UVPD PTCR double-stage fractionation (red) for (A) the window lower and (B) the window higher than the precursor. Spectra were collected with 100 transient averages.

https://doi.org/10.1021/jasms.3c00351
J. Am. Soc. Mass Spectrom. 2024, 35, 255−265

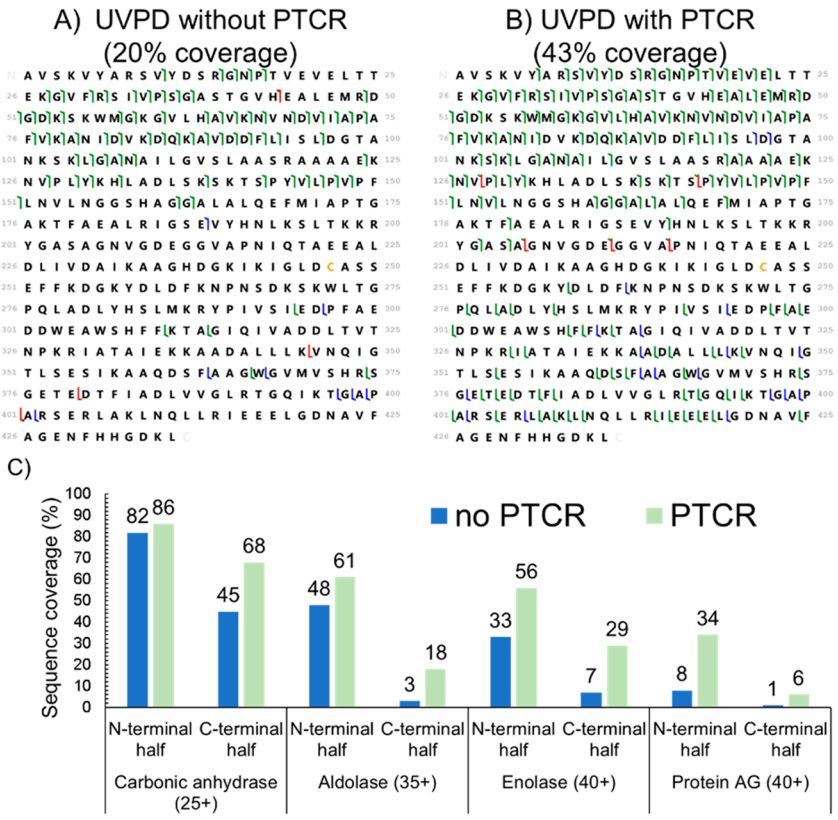

Figure 6. Sequence coverage maps based on UVPD (A) without PTCR and (B) with PTCR of enolase (40+, m/z 1167). PTCR was performed on the entire ion population (no fractionation, so the precursor ion is also subjected to PTCR) with 5−8 injections of the PTCR reagent anion and reaction times of 40−50 ms for each injection. (C) Sequence coverages categorized by N-terminal half or C-terminal half of the protein sequence based on UVPD without or with PTCR of carbonic anhydrase (25+, m/z 1161), aldolase (35+, m/z 1121), enolase (40+, m/z 1167), and protein AG (40+, m/z 1262). The sequence coverage of the N-terminal half is calculated based on those fragment ions originating from cleavages spanning backbone positions 1−129 for carbonic anhydrase, 1−181 for aldolase, 1−218 for enolase, and 1−227 for protein AG. The sequence coverage for the C-terminal half is calculated based on those fragment ions originating from cleavages spanning backbone positions 130−258 for carbonic anhydrase, 182−362 for aldolase, 219−435 for enolase, and 228−453 for protein AG. All spectra were collected with 100 transients averaged and fragment ions were retained only if identified in at least two of three replicates.

highly abundant surviving precursor ion typically present in UVPD spectra may inhibit the detection of these C-terminal ions located in the upper m/z space and likely accounts for the sparse C-terminal coverage for large proteins. This factor underscores the importance of using either fractionation to eliminate the deleterious influence of the nondissociated precursor ion or utilizing PTCR to shift fragment ions away from the nondissociated precursor ion. To illustrate the impact, UVPD was performed on carbonic anhydrase (25+, m/z 1161), aldolase (35+, m/z 1121) enolase (40+, m/z 1167), and protein AG (40+, m/z 1262) without and with PTCR (and without any fractionation). For UVPD with PTCR, the entire ion population was subjected to PTCR using 5−8 injections of the PTCR reagent anion in order to disperse the majority of ions as far as m/z 3000−3500 and simultaneously shift the nondissociated precursor ion population to m/z values higher than that of the majority of fragment ions. Examples of the resulting UVPD and UVPD + PTCR spectra for enolase (40+, m/z 1167) are shown in Figure S20. Sequence coverage maps for enolase (40+) without and with PTCR are displayed in Figure 6A and 6B, respectively, and the maps for the three other proteins are provided in Figure S21. Sequence coverages were evaluated for both the N-terminal and C-terminal halves of each protein as summarized in Figure 6C. Sequence coverages were lower for the C-terminal regions in all cases. PTCR generally improved the sequence coverage of the C-terminal region by a more substantial degree than the N-terminal region. Specifically, sequence coverage of the N-terminal half of proteins increased on average by a factor of 2 whereas the C-terminal half increased by a factor of 5. These trends are consistent with the concept that an abundant precursor ion inhibits the detection of fragment ions higher than it in m/z space, thus suppressing C-terminal coverage.

Throughout this study, typically the lower charge states of proteins were selected for UVPD with the expectation of decreased spectral congestion and ability to trap more protein molecules when using the same AGC target compared to proteins in higher charge states. To evaluate the impact of the precursor charge state, UVPD was performed on the same proteins in higher charge states, including carbonic anhydrase (35+, m/z 830), aldolase (45+, m/z 872), enolase (55+, m/z 849), and protein AG (55+, m/z 918), without and with PTCR (and without any fractionation) to evaluate whether the same trends summarized in Figure 6 were observed for proteins with higher charge densities. The resulting sequence coverage maps are displayed in Figure S22, and sequence coverages for both the N-terminal and C-terminal halves of the four proteins are summarized in Figure S23. Without PTCR, sequence coverages

https://doi.org/10.1021/jasms.3c00351
J. Am. Soc. Mass Spectrom. 2024, 35, 255−265

for these higher charge states were lower owing to more severe spectral congestion. Specifically, the sequence coverages for enolase in the 55+ charge state (m/z 849) were 9% and 22% without and with PTCR, respectively, compared to 20% and 43% without and with PTCR for enolase in the 40+ charge state (m/z 1167). With the exception of protein AG, sequence coverages in the C-terminal halves of the proteins increased by a greater factor than the N-terminal halves when using PTCR. Sequence coverages on average increased by a factor of 2.5 and 3.0 for the N-terminal and C-terminal regions, respectively, for UVPD+PTCR compared to UVPD alone.

CONCLUSIONS

Two main challenges of UVPD of intact proteins include spectral congestion and low signal-to-noise of fragment ions. PTCR has been previously been shown to be highly advantageous in countering spectral congestion when performing UVPD[28] while reducing the risk of false positive identifications.[22] Combining PUF + PTCR with additional fractionation of the fragment ion population further increases the signals of fragment ions while improving confidence in identifications. This extra enhancement upon subfractionation of the fragment ion population is attributed to reduced space charging and dephasing of lower abundance ions. In fact, many of the gains observed with typical PUF + PTCR workflows originate from the fractionation event itself. Notably, fractionation of UVPD spectra reveal that a higher proportion of N-terminal fragment ions are located in the m/z window lower than the precursor while a higher proportion of C-terminal fragment ions are located in the m/z window higher than the precursor. However, the number of proteins analyzed in this study is small, and these trends should be evaluated for a large suite of proteins. Despite the benefits of removing the nondissociated precursor, this population remains an untapped source of additional gains in fragment ion signal. Applying more laser pulses should convert these precursor ions to fragment ions, but primary fragment ions are vulnerable to multiple-generation dissociation and could be transformed into less meaningful products upon exposure to additional laser pulses. Therefore, combining PUF + PTCR fractionation strategies with both ion parking[27,29] and fragment ion protection[23,40] are compelling avenues to further enhance the characterization of intact proteins.

ASSOCIATED CONTENT

Supporting Information

The Supporting Information is available free of charge at https://pubs.acs.org/doi/10.1021/jasms.3c00351.

Evaluation of noise; evaluation of precursor ejection; mass, UVPD and PUF spectra; post-UVPD PTCR double-stage fractionation strategy; sequence coverage data; and fragment ion intensities (PDF)

AUTHOR INFORMATION

Corresponding Author

Jennifer S. Brodbelt − *Department of Chemistry, University of Texas, Austin, Texas 787812, United States;* orcid.org/0000-0003-3207-0217; Email: jbrodbelt@cm.utexas.edu

Author

Sean D. Dunham − *Department of Chemistry, University of Texas, Austin, Texas 787812, United States;* orcid.org/0000-0002-6214-7468

Complete contact information is available at: https://pubs.acs.org/10.1021/jasms.3c00351

Notes

The authors declare the following competing financial interest(s): Christopher Mullen and John Syka are employees of Thermo Fisher Scientific, the developers of the Orbitrap mass spectrometer used for the study. They offered advice and are cited in the Acknowledgements.

ACKNOWLEDGMENTS

We acknowledge the following funding sources: NSF (Grant CHE-2203602) and the Welch Foundation (Grant F-1155). We thank Christopher Mullen and John Syka, both from Thermo Fisher Scientific, Inc., for advice and helpful feedback. We thank Sam Shields for assistance with noise calculations. We acknowledge the repository jPost.[59]

REFERENCES

(1) Donnelly, D. P.; Rawlins, C. M.; DeHart, C. J.; Fornelli, L.; Schachner, L. F.; Lin, Z.; Lippens, J. L.; Aluri, K. C.; Sarin, R.; Chen, B.; Lantz, C.; Jung, W.; Johnson, K. R.; Koller, A.; Wolff, J. J.; Campuzano, I. D. G.; Auclair, J. R.; Ivanov, A. R.; Whitelegge, J. P.; Paša-Tolić, L.; Chamot-Rooke, J.; Danis, P. O.; Smith, L. M.; Tsybin, Y. O.; Loo, J. A.; Ge, Y.; Kelleher, N. L.; Agar, J. N. Best Practices and Benchmarks for Intact Protein Analysis for Top-down Mass Spectrometry. *Nat. Methods* **2019**, *16* (7), 587−594.

(2) Makarov, A.; Eliuk, S. Evolution of orbitrap mass spectrometry instrumentation. *Annual review of analytical chemistry* **2015**, *8*, 61−80.

(3) Tucholski, T.; Ge, Y. Fourier-Transform Ion Cyclotron Resonance Mass Spectrometry for Characterizing Proteoforms. *Mass Spectrom. Rev.* **2022**, *41* (2), 158−177.

(4) Beckman, J. S.; Voinov, V. G.; Hare, M.; Sturgeon, D.; Vasil'ev, Y.; Oppenheimer, D.; Shaw, J. B.; Wu, S.; Glaskin, R.; Klein, C.; Schwarzer, C.; Stafford, G. Improved Protein and PTM Characterization with a Practical Electron-Based Fragmentation on Q-TOF Instruments. *J. Am. Soc. Mass Spectrom.* **2021**, *32* (8), 2081−2091.

(5) Campuzano, I. D. G.; Sandoval, W. Denaturing and Native Mass Spectrometric Analytics for Biotherapeutic Drug Discovery Research: Historical, Current, and Future Personal Perspectives. *J. Am. Soc. Mass Spectrom.* **2021**, *32* (8), 1861−1885.

(6) Brodbelt, J. S. Deciphering Combinatorial Post-Translational Modifications by Top-down Mass Spectrometry. *Curr. Opin. Chem. Biol.* **2022**, *70*, 102180.

(7) Chen, D.; McCool, E. N.; Yang, Z.; Shen, X.; Lubeckyj, R. A.; Xu, T.; Wang, Q.; Sun, L. Recent Advances (2019−2021) of Capillary Electrophoresis-Mass Spectrometry for Multilevel Proteomics. *Mass Spectrom. Rev.* **2023**, *42* (2), 617−642.

(8) Fornelli, L.; Toby, T. K. Characterization of Large Intact Protein Ions by Mass Spectrometry: What Directions Should We Follow? *Biochimica et Biophysica Acta (BBA) - Proteins and Proteomics* **2022**, *1870* (4), 140758.

(9) Melby, J. A.; Roberts, D. S.; Larson, E. J.; Brown, K. A.; Bayne, E. F.; Jin, S.; Ge, Y. Novel Strategies to Address the Challenges in Top-Down Proteomics. *J. Am. Soc. Mass Spectrom.* **2021**, *32* (6), 1278−1294.

(10) Fort, K. L.; Cramer, C. N.; Voinov, V. G.; Vasil'ev, Y. V.; Lopez, N. I.; Beckman, J. S.; Heck, A. J. R. Exploring ECD on a Benchtop Q Exactive Orbitrap Mass Spectrometer. *J. Proteome Res.* **2018**, *17* (2), 926−933.

(11) Riley, N. M.; Mullen, C.; Weisbrod, C. R.; Sharma, S.; Senko, M. W.; Zabrouskov, V.; Westphall, M. S.; Syka, J. E. P.; Coon, J. J. Enhanced Dissociation of Intact Proteins with High Capacity Electron Transfer Dissociation. *J. Am. Soc. Mass Spectrom.* **2016**, *27* (3), 520−531.

(12) Zenaidee, M. A.; Wei, B.; Lantz, C.; Wu, H. T.; Lambeth, T. R.; Diedrich, J. K.; Ogorzalek Loo, R. R.; Julian, R. R.; Loo, J. A. Internal Fragments Generated from Different Top-Down Mass Spectrometry

Fragmentation Methods Extend Protein Sequence Coverage. *J. Am. Soc. Mass Spectrom.* **2021**, *32* (7), 1752−1758.
(13) Riley, N. M.; Westphall, M. S.; Coon, J. J. Sequencing Larger Intact Proteins (30−70 KDa) with Activated Ion Electron Transfer Dissociation. *J. Am. Soc. Mass Spectrom.* **2018**, *29* (1), 140−149.
(14) Shaw, J. B.; Li, W.; Holden, D. D.; Zhang, Y.; Griep-Raming, J.; Fellers, R. T.; Early, B. P.; Thomas, P. M.; Kelleher, N. L.; Brodbelt, J. S. Complete Protein Characterization Using Top-Down Mass Spectrometry and Ultraviolet Photodissociation. *J. Am. Chem. Soc.* **2013**, *135* (34), 12646−12651.
(15) Fornelli, L.; Srzentic, K.; Toby, T. K.; Doubleday, P. F.; Huguet, R.; Mullen, C.; Melani, R. D.; dos Santos Seckler, H.; DeHart, C. J.; Weisbrod, C. R.; Durbin, K. R.; Greer, J. B.; Early, B. P.; Fellers, R. T.; Zabrouskov, V.; Thomas, P. M.; Compton, P. D.; Kelleher, N. L. Thorough Performance Evaluation of 213 Nm Ultraviolet Photodissociation for Top-down Proteomics. *Mol. Cell. Proteomics* **2020**, *19* (2), 405−420.
(16) Gomes, F. P.; Diedrich, J. K.; Saviola, A. J.; Memili, E.; Moura, A. A.; Yates, J. R. EThcD and 213 Nm UVPD for Top-Down Analysis of Bovine Seminal Plasma Proteoforms on Electrophoretic and Chromatographic Time Frames. *Anal. Chem.* **2020**, *92* (4), 2979−2987.
(17) Cannon, J. R.; Cammarata, M. B.; Robotham, S. A.; Cotham, V. C.; Shaw, J. B.; Fellers, R. T.; Early, B. P.; Thomas, P. M.; Kelleher, N. L.; Brodbelt, J. S. Ultraviolet Photodissociation for Characterization of Whole Proteins on a Chromatographic Time Scale. *Anal. Chem.* **2014**, *86* (4), 2185−2192.
(18) Frese, C. K.; Altelaar, A. F. M.; van den Toorn, H.; Nolting, D.; Griep-Raming, J.; Heck, A. J. R.; Mohammed, S. Toward Full Peptide Sequence Coverage by Dual Fragmentation Combining Electron-Transfer and Higher-Energy Collision Dissociation Tandem Mass Spectrometry. *Anal. Chem.* **2012**, *84* (22), 9668−9673.
(19) Greer, S. M.; Sidoli, S.; Coradin, M.; Schack Jespersen, M.; Schwämmle, V.; Jensen, O. N.; Garcia, B. A.; Brodbelt, J. S. Extensive Characterization of Heavily Modified Histone Tails by 193 Nm Ultraviolet Photodissociation Mass Spectrometry via a Middle-Down Strategy. *Anal. Chem.* **2018**, *90* (17), 10425−10433.
(20) Cammarata, M. B.; Thyer, R.; Rosenberg, J.; Ellington, A.; Brodbelt, J. S. Structural Characterization of Dihydrofolate Reductase Complexes by Top-Down Ultraviolet Photodissociation Mass Spectrometry. *J. Am. Chem. Soc.* **2015**, *137* (28), 9128−9135.
(21) Mehaffey, M. R.; Cammarata, M. B.; Brodbelt, J. S. Tracking the Catalytic Cycle of Adenylate Kinase by Ultraviolet Photodissociation Mass Spectrometry. *Anal. Chem.* **2018**, *90* (1), 839−846.
(22) Dunham, S. D.; Wei, B.; Lantz, C.; Loo, J. A.; Brodbelt, J. S. Impact of Internal Fragments on Top-Down Analysis of Intact Proteins by 193 Nm UVPD. *J. Proteome Res.* **2023**, *22* (1), 170−181.
(23) Holden, D. D.; Sanders, J. D.; Weisbrod, C. R.; Mullen, C.; Schwartz, J. C.; Brodbelt, J. S. Implementation of Fragment Ion Protection (FIP) during Ultraviolet Photodissociation (UVPD) Mass Spectrometry. *Anal. Chem.* **2018**, *90* (14), 8583−8591.
(24) Duselis, E. M.; Panepinto, M. C.; Syka, J. E. P.; Mullen, C.; D'Ippolito, R. A.; English, A. M.; Ugrin, S. A.; Shabanowitz, J.; Hunt, D. F. Improved Sequence Analysis of Intact Proteins by Parallel Ion Parking during Electron Transfer Dissociation. *Anal. Chem.* **2021**, *93* (47), 15728−15735.
(25) Stephenson, J. L.; McLuckey, S. A. Ion/Ion Reactions in the Gas Phase: Proton Transfer Reactions Involving Multiply-Charged Proteins. *J. Am. Chem. Soc.* **1996**, *118* (31), 7390−7397.
(26) Kline, J. T.; Mullen, C.; Durbin, K. R.; Oates, R. N.; Huguet, R.; Syka, J. E. P.; Fornelli, L. Sequential Ion-Ion Reactions for Enhanced Gas-Phase Sequencing of Large Intact Proteins in a Tribrid Orbitrap Mass Spectrometer. *J. Am. Soc. Mass Spectrom.* **2021**, *32* (9), 2334−2345.
(27) Weisbrod, C. R.; Anderson, L. C.; Hendrickson, C. L.; Schaffer, L. V.; Shortreed, M. R.; Smith, L. M.; Shabanowitz, J.; Hunt, D. F. Advanced Strategies for Proton-Transfer Reactions Coupled with Parallel Ion Parking on a 21 T FT-ICR MS for Intact Protein Analysis. *Anal. Chem.* **2021**, *93* (26), 9119−9128.
(28) Sanders, J. D.; Mullen, C.; Watts, E.; Holden, D. D.; Syka, J. E. P.; Schwartz, J. C.; Brodbelt, J. S. Enhanced Sequence Coverage of Large Proteins by Combining Ultraviolet Photodissociation with Proton Transfer Reactions. *Anal. Chem.* **2020**, *92* (1), 1041−1049.
(29) Ugrin, S. A.; English, A. M.; Syka, J. E. P.; Bai, D. L.; Anderson, L. C.; Shabanowitz, J.; Hunt, D. F. Ion-Ion Proton Transfer and Parallel Ion Parking for the Analysis of Mixtures of Intact Proteins on a Modified Orbitrap Mass Analyzer. *J. Am. Soc. Mass Spectrom.* **2019**, *30*, 2163−2173.
(30) Xia, Y.; Wu, J.; McLuckey, S. A.; Londry, F. A.; Hager, J. W. Mutual Storage Mode Ion/Ion Reactions in a Hybrid Linear Ion Trap. *J. Am. Soc. Mass Spectrom.* **2005**, *16* (1), 71−81.
(31) Earley, L.; Anderson, L. C.; Bai, D. L.; Mullen, C.; Syka, J. E. P.; English, A. M.; Dunyach, J.-J.; Stafford, G. C.; Shabanowitz, J.; Hunt, D. F.; Compton, P. D. Front-End Electron Transfer Dissociation: A New Ionization Source. *Anal. Chem.* **2013**, *85* (17), 8385−8390.
(32) Anderson, L. C.; English, A. M.; Wang, W.-H.; Bai, D. L.; Shabanowitz, J.; Hunt, D. F. Protein Derivatization and Sequential Ion/Ion Reactions to Enhance Sequence Coverage Produced by Electron Transfer Dissociation Mass Spectrometry. *Int. J. Mass Spectrom.* **2015**, *377*, 617−624.
(33) Walker, J. N.; Lam, R.; Brodbelt, J. S. Enhanced Characterization of Histones Using 193 Nm Ultraviolet Photodissociation and Proton Transfer Charge Reduction. *Anal. Chem.* **2023**, *95* (14), 5985−5993.
(34) McLuckey, S. A.; Reid, G. E.; Wells, J. M. Ion Parking during Ion/Ion Reactions in Electrodynamic Ion Traps. *Anal. Chem.* **2002**, *74* (2), 336−346.
(35) Holden, D. D.; McGee, W. M.; Brodbelt, J. S. Integration of Ultraviolet Photodissociation with Proton Transfer Reactions and Ion Parking for Analysis of Intact Proteins. *Anal. Chem.* **2016**, *88* (1), 1008−1016.
(36) Chrisman, P. A.; Pitteri, S. J.; McLuckey, S. A. Parallel Ion Parking of Protein Mixtures. *Anal. Chem.* **2006**, *78* (1), 310−316.
(37) Bailey, A. O.; Huguet, R.; Mullen, C.; Syka, J. E. P.; Russell, W. K. Ion-Ion Charge Reduction Addresses Multiple Challenges Common to Denaturing Intact Mass Analysis. *Anal. Chem.* **2022**, *94* (9), 3930−3938.
(38) Huguet, R.; Mullen, C.; Srzentić, K.; Greer, J. B.; Fellers, R. T.; Zabrouskov, V.; Syka, J. E. P.; Kelleher, N. L.; Fornelli, L. Proton Transfer Charge Reduction Enables High-Throughput Top-Down Analysis of Large Proteoforms. *Anal. Chem.* **2019**, *91* (24), 15732−15739.
(39) Payne, A. H.; Glish, G. L. Thermally Assisted Infrared Multiphoton Photodissociation in a Quadrupole Ion Trap. *Anal. Chem.* **2001**, *73* (15), 3542−3548.
(40) Dunham, S. D.; Sanders, J. D.; Holden, D. D.; Brodbelt, J. S. Improving the Center Section Sequence Coverage of Large Proteins Using Stepped-Fragment Ion Protection Ultraviolet Photodissociation. *J. Am. Soc. Mass Spectrom.* **2022**, *33* (3), 446−456.
(41) Chrisman, P. A.; Pitteri, S. J.; McLuckey, S. A. Parallel Ion Parking: Improving Conversion of Parents to First-Generation Products in Electron Transfer Dissociation. *Anal. Chem.* **2005**, *77* (10), 3411−3414.
(42) Weisbrod, C. R.; Kaiser, N. K.; Syka, J. E. P.; Early, L.; Mullen, C.; Dunyach, J.-J.; English, A. M.; Anderson, L. C.; Blakney, G. T.; Shabanowitz, J.; Hendrickson, C. L.; Marshall, A. G.; Hunt, D. F. Front-End Electron Transfer Dissociation Coupled to a 21 T FT-ICR Mass Spectrometer for Intact Protein Sequence Analysis. *J. Am. Soc. Mass Spectrom.* **2017**, *28* (9), 1787−1795.
(43) Weisbrod, C. R.; Anderson, L. C.; Greer, J. B.; DeHart, C. J.; Hendrickson, C. L. Increased Single-Spectrum Top-Down Protein Sequence Coverage in Trapping Mass Spectrometers with Chimeric Ion Loading. *Anal. Chem.* **2020**, *92* (18), 12193−12200.
(44) Prentice, B. M.; Ryan, D. J.; Grove, K. J.; Cornett, D. S.; Caprioli, R. M.; Spraggins, J. M. Dynamic Range Expansion by Gas-Phase Ion Fractionation and Enrichment for Imaging Mass Spectrometry. *Anal. Chem.* **2020**, *92* (19), 13092−13100.
(45) Dayon, L.; Sonderegger, B.; Kussmann, M. Combination of Gas-Phase Fractionation and MS3 Acquisition Modes for Relative Protein

https://doi.org/10.1021/jasms.3c00351
J. Am. Soc. Mass Spectrom. 2024, 35, 255−265

Quantification with Isobaric Tagging. *J. Proteome Res.* **2012**, *11* (10), 5081−5089.
(46) Meier, F.; Geyer, P. E.; Winter, S. W.; Cox, J.; Mann, M. BoxCar acquisition method enables single-shot proteomics at a depth of 10,000 proteins in 100 minutes. *Nat. Methods* **2018**, *15*, 440−448.
(47) Klaeger, S.; Apffel, A.; Clauser, K. R.; Sarkizova, S.; Oliveira, G.; Rachimi, S.; Le, P. M.; Tarren, A.; Chea, V.; Abelin, J. G.; Braun, D. A.; Ott, P. A.; Keshishian, H.; Hacohen, N.; Keskin, D. B.; Wu, C. J.; Carr, S. A. Optimized Liquid and Gas Phase Fractionation Increases HLA-Peptidome Coverage for Primary Cell and Tissue Samples. *Molecular & Cellular Proteomics* **2021**, *20*, 100133.
(48) Hebert, A. S.; Prasad, S.; Belford, M. W.; Bailey, D. J.; McAlister, G. C.; Abbatiello, S. E.; Huguet, R.; Wouters, E. R.; Dunyach, J.-J.; Brademan, D. R.; Westphall, M. S.; Coon, J. J. Comprehensive Single-Shot Proteomics with FAIMS on a Hybrid Orbitrap Mass Spectrometer. *Anal. Chem.* **2018**, *90* (15), 9529−9537.
(49) Hofmann, A. E.; Chimiak, L.; Dallas, B.; Griep-Raming, J.; Juchelka, D.; Makarov, A.; Schwieters, J.; Eiler, J. M. Using Orbitrap Mass Spectrometry to Assess the Isotopic Compositions of Individual Compounds in Mixtures. *Int. J. Mass Spectrom.* **2020**, *457*, 116410.
(50) Holden, D. D.; Brodbelt, J. S. Improving Performance Metrics of Ultraviolet Photodissociation Mass Spectrometry by Selective Precursor Ejection. *Anal. Chem.* **2017**, *89* (1), 837−846.
(51) Shields, S. W. J.; Sanders, J. D.; Brodbelt, J. S. Enhancing the Signal-to-Noise of Diagnostic Fragment Ions of Unsaturated Glycerophospholipids via Precursor Exclusion Ultraviolet Photodissociation Mass Spectrometry (PEx-UVPD-MS). *Anal. Chem.* **2022**, *94* (32), 11352−11359.
(52) Makarov, A.; Denisov, E. Dynamics of Ions of Intact Proteins in the Orbitrap Mass Analyzer. *J. Am. Soc. Mass Spectrom.* **2009**, *20* (8), 1486−1495.
(53) Klein, D. R.; Holden, D. D.; Brodbelt, J. S. Shotgun Analysis of Rough-Type Lipopolysaccharides Using Ultraviolet Photodissociation Mass Spectrometry. *Anal. Chem.* **2016**, *88* (1), 1044−1051.
(54) Mullen, C.; Weisbrod, C. R.; Syka, J. E. P. Methods of Performing Ion-ion Reactions in Mass Spectrometry. *US Patent* **2018**, 9991107B2.
(55) Kostelic, M. M.; Zak, C. K.; Liu, Y.; Chen, V. S.; Wu, Z.; Sivinski, J.; Chapman, E.; Marty, M. T. UniDecCD: Deconvolution of Charge Detection-Mass Spectrometry Data. *Anal. Chem.* **2021**, *93* (44), 14722−14729.
(56) Zhurov, K. O.; Kozhinov, A. N.; Fornelli, L.; Tsybin, Y. O. Distinguishing Analyte from Noise Components in Mass Spectra of Complex Samples: Where to Cut the Noise? *Anal. Chem.* **2014**, *86* (7), 3308−3316.
(57) Olsen, J. V.; de Godoy, L. M. F.; Li, G.; Macek, B.; Mortensen, P.; Pesch, R.; Makarov, A.; Lange, O.; Horning, S.; Mann, M. Parts per Million Mass Accuracy on an Orbitrap Mass Spectrometer via Lock Mass Injection into a C-Trap. *Mol. Cell. Proteomics* **2005**, *4* (12), 2010−2021.
(58) Grinfeld, D. E.; Kopaev, I. A.; Makarov, A. A.; Monastyrskiy, M. A. Equilibrium Ion Distribution Modeling in RF Ion Traps and Guides with Regard to Coulomb Effects. *Nuclear Instruments and Methods in Physics Research Section A: Accelerators, Spectrometers, Detectors and Associated Equipment* **2011**, *645* (1), 141−145.
(59) Okuda, S.; Watanabe, Y.; Moriya, Y.; Kawano, S.; Yamamoto, T.; Matsumoto, M.; Takami, T.; Kobayashi, D.; Araki, N.; Yoshizawa, A. C.; Tabata, T.; Sugiyama, N.; Goto, S.; Ishihama, Y. jPOSTrepo: an international standard data repository for proteomes. *Nucleic Acids Res.* **2017**, *45*, D1107−D1111.

https://doi.org/10.1021/jasms.3c00351
J. Am. Soc. Mass Spectrom. 2024, 35, 255−265